Structure of Shock Waves and Inelasticity in Shock-Compressed Cemented Tungsten Carbides

Bingsen Wang and Vikas Prakash
Institute for Shock Physics
Washington State University, Pullman, WA 99164

ABSTRACT
In the present study, shock wave experiments are conducted on General Carbide cemented tungsten carbide with 3.7wt.% cobalt binder to determine its shock-induced compression behavior up to 100 GPa. The measured wave profiles indicate the cemented tungsten carbide to undergo elastic-plastic deformation during shock compression. A three-stage particle velocity profile is observed in the experiments -- an initial elastic-rise to the Hugoniot Elastic Limit (HEL), an elastic-plastic ramp indicating substantial post-yield hardening, and finally a rise to the peak shocked Hugoniot state. The results of the experiments are used to determine the HEL, the shock velocity (U_s) vs. particle velocity (u_p) Hugoniot relation, and the longitudinal stress (σ_x) vs. specific volume (V) curve for the samples. The HEL of the material was determined to lie between 4.41 GPa and 4.58 GPa. The $U_s - u_p$ relation was determined to be $U_s = 4.97 + 1.457u_p$ for particle velocities greater than 0.75 km/s. The measured plastic shock velocities for particle velocities less than 0.7 km/s were found to be larger than those predicted using the linear $U_s - u_p$ Hugoniot relationship, indicating the cemented WC samples to preserve substantial shear strength in the post-yield deformation region. No phase transformation was observed up to 100 GPa.

Keywords: Cemented tungsten carbide, normal shock compression, shock profiles, in-material Hugoniot quantities

INTRODUCTION

Cemented tungsten carbides are metal matrix composites in which a large fraction of hard tungsten carbide (WC) grains is embedded in a soft transition metal matrix, e.g., cobalt, nickel, iron, etc., commonly referred to as the binder. A compromise of high hardness and toughness is achieved by optimizing the composition of the primary constituents (i.e., WC grains and the binder), and the material microstructure. Because of their high density and hardness, these composites have been particularly attractive in applications where high-rate mechanical loading, high hardness, and high wear resistance is important. However, to date, very little fundamental information is available on their shock and impact properties in the open literature [1-3].

The primary objective of the present work is to better understand the structure of shock waves and their associated thermodynamic equilibrium states in shock-compressed cemented WC with 3.7 wt. % Co binder. The peak shocked state of interest to this study is up to 100 GPa, which is more than fifteen times the Hugoniot Elastic Limit (HEL) reported for WC ceramics in the literature [4]. Besides calculation of in-material quantities in the elastic-limit and the peak shocked Hugoniot states, Hugoniot relations for the cemented WC sample in terms of the shock velocity vs. particle velocity ($U_s - u_p$) and longitudinal stress vs volume compression ($\sigma_x - V/V_o$) are determined over the stress range of interest.

EXPERIMENTAL METHODS

Cemented tungsten carbide samples with 3.7 wt. % cobalt binder were obtained from General Carbide, PA. The samples were manufactured by powder metallurgy where tungsten carbide powder is mixed with the binder metal, compacted in a die, and then sintered in a furnace. The process results in cementing the tungsten grain particles with the metallic binder, forming a strong metallurgical bond between the tungsten carbide grains and the metal binder. During sintering, the microstructure of the WC cermet samples was controlled such that the average grain size lies in a narrow band of 1 to 2 microns. All samples were characterized by density and sound speed measurements at ambient conditions. The physical properties of the cemented WC samples are presented in Table I.

Table I: Physical properties of General Carbide cemented WC- 3.7 wt.% cobalt.

Physical Properties	
Density (g/cm^3)	15.17
Bulk Modulus (GPa)	375.1
Poisson's ratio	0.209
Longitudinal wave speed (km/s)	6.97
Shear wave speed (km/s)	4.23
Bulk wave speed (km/s)	4.97

A summary of the shock experiments conducted in the present study is provided in Table II. The table lists the Shot number, driver used, impact velocity, the impactor and buffer materials, peak stress attained, and the estimated impact tilt in each experiment. A schematic of the experimental configuration is shown in Fig. 1. Experiments at peak stress higher than 15.66 GPa (Shots 01, 02, 03, 04, 05 and 08) were conducted using a 30 mm powder gun, while experiments at peak stress of 8.97 and 15.66 GPa (Shots 06 and 07) were conducted using the 100 mm single stage light gas gun at the Institute for Shock Physics, Washington State University. Typical impactor and target plate assembly for the low peak stress experiments (Shots 06 and 07), comprised an Al-1050 impactor, a-cut sapphire buffer that is bonded to the cemented WC sample, and a $< 100 >$ LiF window. For the intermediate peak stress experiments (Shot 08) an Al-1050 impactor, Al-1050 buffer bonded to the WC sample, and a LiF window was used. For the higher peak stress experiments (Shots 01 to 05) the impactor and the buffer materials in the intermediate peak stress configuration were replaced by C-101 copper. The use of the same impactor and the buffer materials in the experiments help to limit wave interactions due to wave reflections at the impactor/buffer interface. Prior to bonding the various target components, a thin aluminum mirror is vapor deposited onto the front surface of the LiF window, which served as a reflector for laser interferometry (VISAR-Velocity Interferometer System for Any Reflector) measurements [5-7]. In all experiments, the VISAR measurements used a dual velocity-per-fringe configuration to unambiguously determine the peak particle velocity [8]. The central VISAR probe, shown by the red arrow in Fig. 1, provides the shock wave transit times through the sample along with the particle velocity profiles at the WC sample/window interface. The three (outer) radial VISAR probes (Fig. 1 – black arrows), focused on the back of the polished buffer at 120° intervals, allow determination of the shock arrival times at the sample/buffer interface and the impact tilt in the experiments. The maximum impact tilt in the experiments was estimated to be 1.9 mrad.

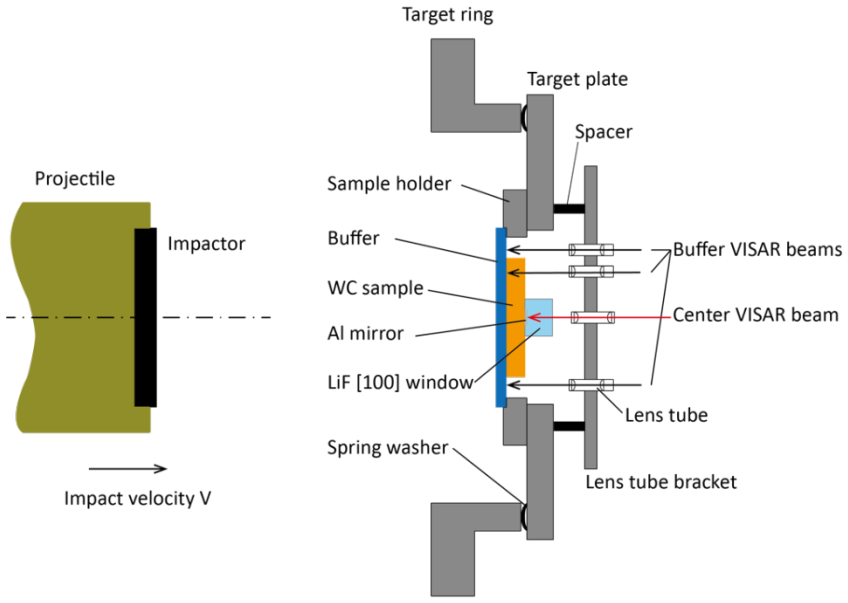

Figure 1: Schematic of the experimental configuration used in the present experiments.

Table II: Summary of plate impact experiments conducted on the cemented WC-3.7 wt.% Co samples used in the present experiment. In all experiments, the elastic shock wave in the buffer was overdriven by the plastic shock wave.

Shot #	Driver	Impact Vel. (km/s)	WC Sample Thickness (mm)	Impactor/ Thickness (mm)	Buffer/ Thickness (mm)	Window/ Thickness (mm)	Peak Stress (GPa)	Impact Tilt (mrad)
01 (103-01)	30 mm powder gun	1.400	2.588	C101-Cu/ 1.707	C101-Cu/ 1.072	⟨100⟩ LiF/ 6.389	42.98	1.12
02 (103-03R)	30 mm powder gun	2.667	2.565	C101-Cu/ 1.710	C1011-Cu/ 1.132	⟨100⟩ LiF/ 6.397	94.13	1.22
03 (103-04)	30 mm powder gun	1.695	2.566	C101-Cu/ 1.733	C101-Cu/ 1.115	⟨100⟩ LiF/ 6.384	53.77	0.73
04 (103-05)	30 mm powder gun	2.360	2.571	C101-Cu/ 1.718	C101-Cu/ 1.124	⟨100⟩ LiF/ 6.402	80.42	1.59
05 (103-06)	30 mm powder gun	1.994	2.572	C101-Cu/ 1.743	C101-Cu/ 1.132	⟨100⟩ LiF/ 6.391	65.78	1.90
06 (103-07)	100 mm gas gun	0.545	2.558	Al-1010/ 2.336	a-cut Sapphire/ 3.191	⟨100⟩ LiF/ 6.385	8.97	0.57
07 (103-08)	100 mm gas gun	0.909	2.562	Al-1010/ 2.378	a-cut Sapphire/ 3.191	⟨100⟩ LiF/ 6.389	15.66	1.12
08 (103-09)	30 mm powder gun	1.818	2.564	Al-1010/ 2.528	Al-1010/ 0.984	⟨100⟩ LiF/ 6.389	29.25	0.65

WAVE PROPAGATION IN THE FLYER AND TARGET ASSEMBLY: LAGRANGIAN TIME -- DISTANCE DIAGRAM

For the high peak stress experiments, the copper (buffer)−WC (sample)−LiF (window) target assemblies were impacted with copper impactors, launched using a light powder gun. Upon impact, a single overdriven shock wave propagates into the copper buffer and impactor. The forward propagating shock in the buffer interacts with the buffer/sample interface, resulting in both elastic and plastic shock waves to propagate through the WC sample and a reflected re-shock wave travelling backwards into the buffer. Due to the impedance contrast between the sample and the window, the propagating elastic and plastic waves in the WC sample undergo further transmission and reflection at the WC sample/window interface. The shock wave in the impactor eventually reaches its back surface and reflects from it as a rarefaction wave. The corresponding Lagrangian time vs distance diagram is shown in Fig. 2.

For the low and intermediate peak stress experiments, the copper impactor is replaced by Al-1010 while the buffer is replaced by either a-cut sapphire (Shots 06 and 07) or Al-1010 (Shot 08). For the impact configuration used in Shots 06 and 07, a two-wave structure is developed in the impactor while only a single elastic shock wave is generated in the a-cut sapphire, which loads the sample.

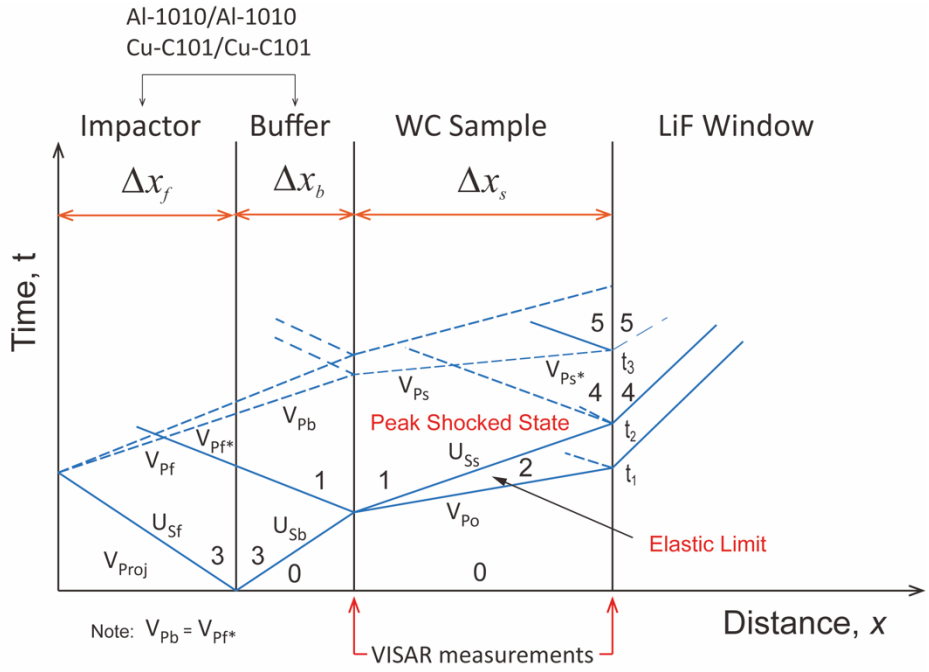

Figure 2: Lagrangian distance-time diagram for the high impact experiments conducted in the present study. U_s is shock velocity, V_P is the compressional sound velocity and V_{Po} is the elastic precursor velocity and t_1, t_2 and t_3 are wave arrival times at the sample-window interface. The subscripts *f*, *b* and *s* refer to the flyer, buffer, and sample, respectively.

EXPERIMENTAL RESULTS

Eight normal shock compression plate impact experiments were conducted on the cemented tungsten carbide samples in the present study. These experiments were designed to impart peak stress levels in the range 8.97 GPa to 94.13 GPa in the shocked state. The experimental parameters relevant to these eight experiments are summarized in Table II. The intermediate and high Hugoniot (peak) stress plate impact experiments were conducted using a 30 mm bore powder gun, while the low peak stress experiments were conducted using the 100 mm single-stage gas-gun facility at the Institute for Shock Physics, Washington State University. For the low peak stress experiments, a-axis sapphire (HEL ~ 18 GPa) is used as the buffer with Al-1050 as the impactor, while for the intermediate and high peak stress experiments either Al-1050 or OFE Cu plates were employed as both impactor and buffer plates. In all experiments, a $< 100 >$ LiF window is used behind the WC sample. Projectile velocities were chosen such that the elastic wave in the buffer is overdriven and a single shock wave is incident at the buffer/WC sample interface, resulting in a constant peak stress state in the WC samples.

Figure 3 shows the wave profiles measured at the sample/window interface using VISAR interferometry. In all experiments, a two-wave structure comprising an elastic precursor and a trailing plastic wave is observed. The elastic precursor amplitude (HEL) is nearly constant (within the experimental scatter) at all impact velocities [9]. No yield drop (stress relaxation) immediately behind the elastic wave front is observed in the particle velocity profiles. Beyond the HEL the longitudinal stress rises continuously to the peak stress state, with the rate of increase in stress being higher for larger stress in the peak state. The quantitative measurement of primary interest to this work is the particle velocity at the sample/window interface at the elastic limit (corresponding to the Hugoniot Elastic Limit), and the peak stress state, from which the in-material Hugoniot properties can be calculated [10-12].

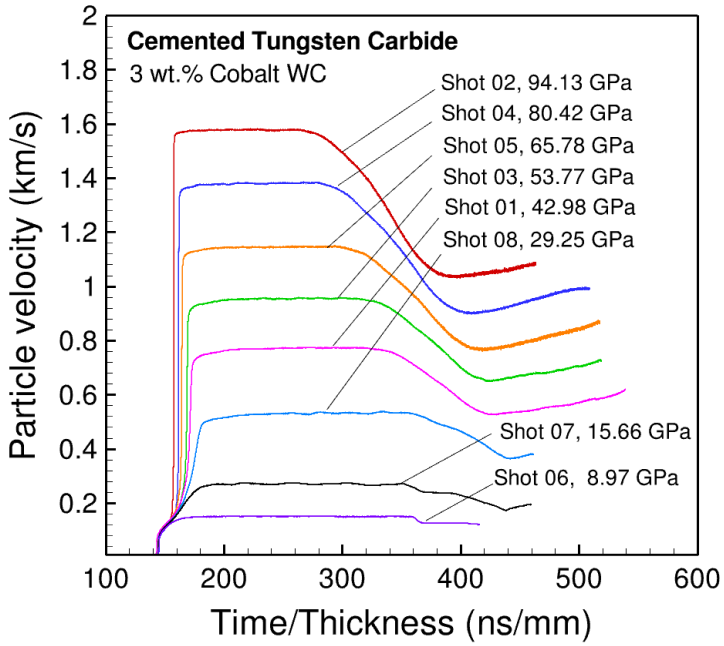

Figure 3: Measured particle velocity profiles at the WC/LiF window for WC samples shocked up to 100 GPa. Time is normalized with the sample thickness.

ANALYSIS

Figure 4 shows the longitudinal stress vs particle velocity diagram for a typical experiment conducted using a copper impactor and copper buffer combination in the present study. A two-wave structure is considered in the analysis of the Hugoniot states in the WC samples -- elastic limit behind the leading elastic precursor and a peak shocked state behind the trailing plastic shock wave. The objective of the analysis is to calculate the in-material Hugoniot quantities of interest (i.e., longitudinal stress, particle velocity, elastic shock wave speed and density compression) in the elastic limit (State 2) and the peak shocked state (State 1) using impedance matching procedures and the Rankine-Hugoniot jump conditions. The principal Hugoniot ($U_s - u_p$) relations for the impactor, buffer and the window used in the calculations are summarized in Table III.

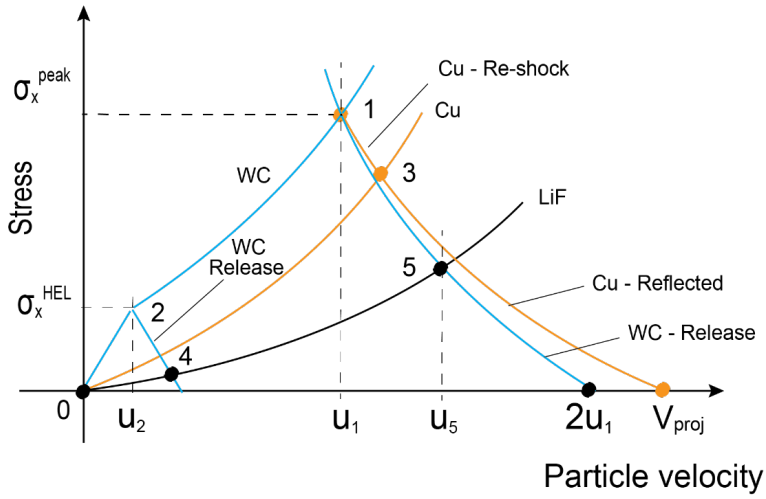

Figure 4: Stress vs. Particle velocity diagram showing the various Hugoniot shock and release states achieved in the WC sample, impactor and the buffer plates in a typical shock experiment.

Table III: Hugoniot $U_s - u_p$ relationship for the impactor, buffer and window materials used in the present study.

Material	$U_s - u_p$ **Hugoniot**
Cu-C101	$U_s = 3.97 + 1.479\, u_p$
Al-1050	$U_s = 5.35 + 1.32\, u_p$
a-cut Sapphire	$U_s = 11.213 + 0.97\, u_p$
LiF $< 100 >$	$U_s = 5.215 + 1.351\, u_p$

To facilitate the calculation of the in-material quantities at the elastic limit and peak stress state, the cemented WC samples were idealized as rate independent, elastic perfectly plastic materials; accordingly, the measured particle velocity profiles were idealized as a two-step function. Because of this assumption, time dependence of material behavior on the structure of the shock waves was not considered in the present analysis.

For $\sigma_x \leq \sigma_x^{HEL}$

Since the material ahead of the elastic precursor in the WC samples is stationary, the Eulerian elastic shock wave speed in the sample, $D_{0\to2}$, is the same as the Lagrangian (measured) elastic shock wave speed $D_{0\to2}^{L} = \Delta x_s/(t_1 - t_0)$, where Δx_s represents the un-deformed thickness of the WC sample and $(t_1 - t_{0)}$ is the transit time of the elastic shock wave in the sample.

Using the $\sigma - u$ Hugoniot relationship connecting States 0 and 2 in WC, gives

$$\sigma_{x2}^{HEL} = \rho_0^{WC}\, D_{0\to2} u_2 = \rho_0^{WC} D_{0\to2}^{L} u_2 \tag{1}$$

where, σ_{x2}^{HEL} is the peak stress at the elastic limit, ρ_0^{WC} is the (ambient) density of the WC sample in State 0, and u_2 is the particle velocity in State 2.

The longitudinal stress in the shocked WC after release at the WC/LiF interface (State 4) gives

$$\sigma_{x4} = \rho_0^{WC} D_{0\to2}^{L}(2u_2 - u_4) \tag{2}$$

In Eq (2), σ_{x4} and u_4 are the longitudinal stress and particle velocity states in State 4 at the WC/LiF window interface.

Moreover, principal Hugoniot for shocked LiF connecting State 0 to 4, gives

$$\sigma_{x4} = \rho_0^{LiF}(A^{LiF} + B^{LiF}\, u_4)u_4 \tag{3}$$

where, ρ_0^{LiF} is the ambient density of LiF in State 0, and $A^{LiF}$and B^{LiF} are the known $U_s - u_p$ Hugoniot parameters for LiF.

Conservation of mass for shocked WC from State 0 to State 2, gives

$$\rho_0^{WC}\, D_{0\to2} = \rho_2^{WC}(D_{0\to2} - u_2) \tag{4}$$

Using Eqs. (1) to (4) along with the measured particle velocity at the WC/LiF window interface, the longitudinal stress at the elastic limit σ_{x2}^{HEL}, material density ρ_2^{WC}, and the particle velocity u_2, can be calculated.

For $\sigma_x > \sigma_x^{HEL}$

The Lagrangian plastic shock wave speed in the shocked WC, $D_{2\to1}^{L}$, can be expressed as

$$D_{2\to1}^{L} = \frac{\Delta x_s}{(t_2 - t_0)} \tag{5}$$

where $(t_2 - t_{0)}$ is the transit time of the plastic shock wave in the shocked sample.

Accordingly, the Eulerian plastic shock wave speed connecting the elastic limit (State 2) to the peak shocked state (State 1) in the WC samples, i.e., $D_{2\to1}$, can be written as

$$D_{2\to1} = u_2 + \frac{\rho_0^{WC}}{\rho_2^{WC}} D_{2\to1}^{L} \tag{6}$$

Using the $\sigma - u$ Hugoniot relationship for shocked WC, the longitudinal stress σ_{x1} in the peak stress state can be expressed in terms of the measured plastic shock wave speed $D_{2\to1}^{L}$ and the particle velocity u_1, as

$$\sigma_{x1} - \sigma_{x2}^{HEL} = \rho_2^{WC}(\, D_{2\to1} - u_2\,)(u_1 - u_2) = \rho_0^{WC} D_{2\to1}^{L}(u_1 - u_2) \tag{7}$$

To calculate the particle velocity u_1 in the peak stress state (State1), consider plastic release of the shocked WC from State 1 to State 5 (at the LIF/WC window interface) using the reflected Hugoniot from State 1. Using the principal Hugoniot for shocked LiF connecting State 0 to 5, the longitudinal stress at the WC/LiF interface can be expressed as

$$\sigma_{x5} = \rho_0^{WC} D_{2\to1}^{L}(2u_1 - u_5) = \rho_0^{LiF}(A^{LiF} + B^{LiF}u_5)u_5 \tag{8}$$

Also, considering elastic release of WC from State 1 to State 5, the stress at the WC/LiF window interface can be expressed as

$$\sigma_{x5} = \rho_0^{WC} D_{2\to1}^{L}(u_1 - u_2) + \sigma_{x2}^{HEL} - \rho_0^{WC} D_{0\to2}^{L}(u_5 - u_1) = \rho_0^{LiF}(A^{LiF} + B^{LiF}u_5)u_5 \tag{9}$$

Then, the particle velocity u_1 at the peak stress state (State 1) is then taken to be the average of the two values calculated using Eqs. (8) and (9). Knowing u_1, the peak stress in State 1 can be calculated.

Also, conservation of mass in the shocked WC between States 1 and 2, gives

$$\rho_2^{WC}(\, D_{2\to1} - u_2) = \rho_1^{WC}(D_{2\to1} - u_1) \tag{10}$$

Using Eqs. (5) to (10) and the measured particle velocity at the WC/LiF window interface, the longitudinal stress, σ_{x1}, material density, ρ_1^{WC}, and the particle velocity, u_1, can be calculated in the peak stress state in the WC samples.

The calculated in-material quantities at both the elastic limit and the peak stress state in the cemented WC samples are summarized in Table IV.

Table IV: In-material quantities in shocked cemented WC samples at the elastic limit and the peak stress state calculated using impedance matching procedures and the measured particle velocity at the WC/LiF window interface. Note $D_{0\to2}$ and $D_{2\to1}^{L}$ are the measured elastic and plastic shock wave speeds, respectively, and $D_{2\to1}$ is the Eulerian plastic wave speed.

Shot #	**Impact Vel. (km/s)**	**Wave Speeds**			**Elastic Limit**			**Peak Shocked State**		
		$D_{0\to2}$ **(km/s)**	$D_{2\to1}$ **(km/s)**	$D_{2\to1}^{L}$ **(km/s)**	**Stress (GPa)**	**Density (GPa)**	**Particle Vel. (km/s)**	**Stress (GPa)**	**Density (GPa)**	**Particle Vel. (km/s)**
01 (103-01)	1.40	6.9862	5.8659	5.8590	4.5804	15.2545	0.0433	42.9788	16.4222	0.4756
02 (103-03R)	2.667	6.9338	6.3671	6.3635	4.6222	15.2972	0.0440	94.1319	17.9350	0.9716
03 (103-04)	1.695	6.9712	5.9537	5.9476	4.4057	15.2310	0.0417	53.7652	16.7833	0.5892
04 (103-05)	2.360	6.8962	6.1904	6.1816	4.4506	15.2642	0.0426	80.4193	17.5809	0.8524
05 (103-06)	1.994	6.9788	6.0906	6.0850	4.6108	15.2553	0.0436	65.7804	17.1343	0.7067
06 (103-07)	0.545	6.9000	6.5880	6.5860	4.6212	15.2877	0.0441	8.9681	15.3899	0.0875
07 (103-08)	0.909	6.8988	6.1466	6.1419	4.5028	15.2952	0.0429	15.6624	15.6008	0.1625
08 (103-09)	1.818	6.9446	5.8463	5.8391	4.5454	15.2655	0.0433	29.2480	16.0507	0.3247

RESULTS AND DISCUSSION

Details of the measured particle velocity profiles immediately following the elastic precursor and preceding the attainment of final peak stress state for all experiments in the present study, are shown in Fig. 5. The wave profiles show a diffused change in slope in the particle velocity profiles in the stress range 4.41 GPa to 4.581 GPa. This change in slope is identified as the HEL for the WC cermet used in the present investigation. The average stress at HEL is calculated to be 4.52 GPa. Since the precision for measurements of particle and free surface velocity is 1-2%, the statistical uncertainty associated with the average value of the HEL is likely to arise from the variability in the material microstructure.

Following the elastic precursor, a distinct ramp in the measured particle velocity is observed in all experiments. This ramp in particle velocity is followed by a relatively sharp increase in particle velocity at ca. 0.165 km/s. This sudden change in particle velocity following the ramp occurs at ca. 7 GPa, which is approximately equal to the HEL of pure WC ceramics. Similar features in the measured particle velocity profiles immediately following the HEL in shocked cemented WCs with cobalt and nickel binders were noted by Grady [13] and Appleby-Thomas [14], where they attributed the initial break in particle velocity to elastic limit of the cemented WC and the second sharper break (rise) in particle velocity to the elastic limit of the WC grains comprising the material microstructure. The shock waves following the second break in particle velocity travel in the shocked cemented WC samples with velocities in the range 5.839 km/s and 6.586 km/s. These Eulerian shock velocities are much higher than the bulk sound wave speed in the cemented WC at ambient conditions, i.e., 4.97 km/s, suggesting the role of pressure and the associated density compression in the shocked cemented WC samples.

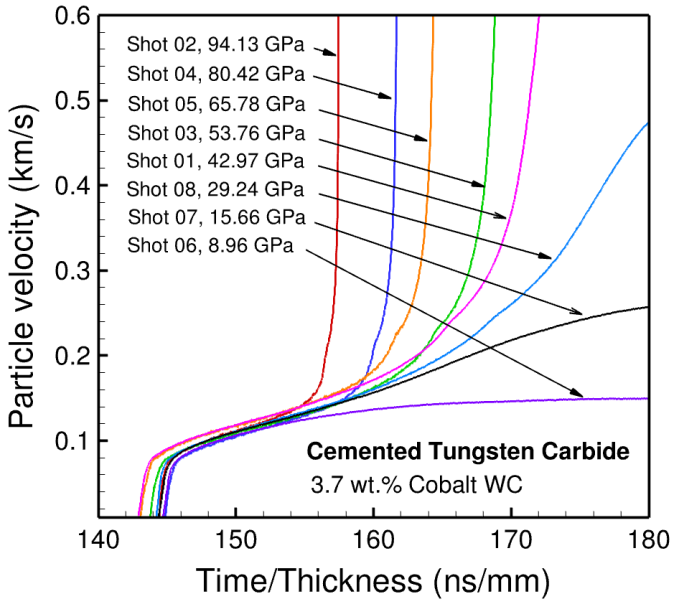

Figure 5: Precursor characteristics of General Carbide cemented WC with 3.7 wt.% cobalt binder.

The shock speed vs. particle velocity relation for cermet WC--3.7 wt.% Co binder is shown in Fig. 6 together with the ultrasonic wave speed data and the results of shock wave experiments by McQueen *et al.* [15] on WC-- 5 wt.% Co binder. The measured elastic shock wave speeds in the cemented WC samples used in the present study were consistent with the zero-pressure longitudinal sound velocity obtained from ultrasonic measurements, as shown in Table IV. In the plastic region, the shock velocities were much larger compared with the bulk sound velocity, and for those less than 0.75km/s particle velocity were further larger than the linear Hugoniot relation. In addition, the shock velocities decrease with the increase in particle velocity below 0.75 km/s -- indicating that the samples preserve a high shear strength in the post-HEL plastic region.

The $U_s - u_p$ curve for cemented WC -- 3.7 wt.% cobalt was obtained by following an approach similar to the one used in their work by McQueen *et al.* [15] on cemented WC -- 5% cobalt binder. The density of the samples used by McQueen et al. was 15.01 g/cm^3. The longitudinal and shear wave velocities were reported to be 6.89 km/s and 4.18 km/s, respectively. The

calculated bulk sound wave speed and Poisson's ratio were 4.92 km/s and 0.209, respectively. These values are not very different from the measured values of sound speeds in the WC--3.7 wt. % cobalt samples used in the present study. Careful examination of the experimental data in Fig. 5 and considering that hydrodynamic equilibrium in the shocked cemented WC samples is not attained until longitudinal stress of ca. 75 GPa, yields the following linear relation between the shock velocity (U_s) and the particle velocity (u_p) for particle velocities greater than 0.75 km/s

$$U_s = 4.97 + 1.457\, u_p \tag{10}$$

In deriving this equilibrium $U_s - u_p$ Hugoniot relation, the intercept of the Hugoniot fit is forced to coincide with the bulk sound speed obtained from the measured longitudinal and shear wave speeds; the slope of the U_s - u_p relation is determined by the high-stress data alone.

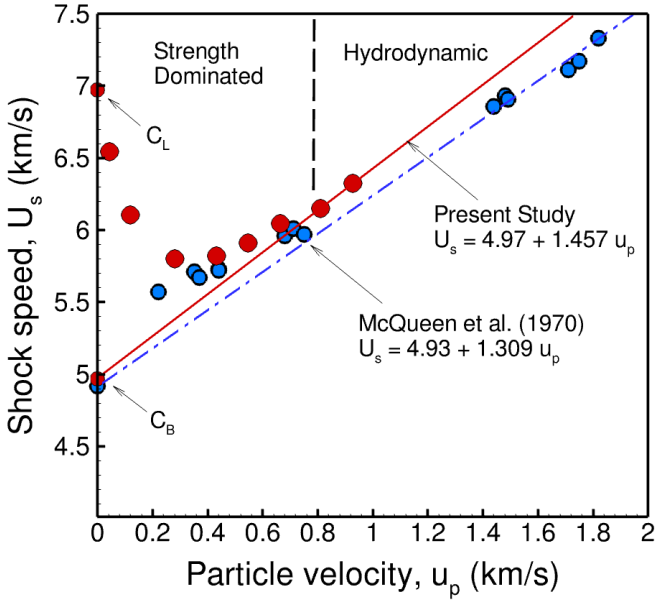

Figure 6: Shock speed vs. particle velocity Hugoniot relation for cemented WC-- 3.7 wt.% cobalt (present work) and WC --5 wt.% cobalt (McQueen *et al.* [15]).

The experimental Hugoniot-compression data for General Carbide cemented WC -- 3.7 wt. % Co used in the present study, WC--5 wt. % Co used by McQueen et al., and Cercom pure WC ceramic used in their work by Dandekar and Grady [4] are shown along with their calculated hydrodynamic-compression curves in Fig. 7. The hydrodynamic compression curves were calculated using the bulk modulus 375.1 GPa with s = 1.42 (present work) and bulk modulus 363.33 GPa with s = 1.309 for the case of WC samples used by McQueen et al. [15] and by Dandekar and Grady [4]. The Hugoniot data from the present work and from McQueen et al. falls on their respective hydrodynamic-compression curves for longitudinal stresses greater than ca. 75 GPa, while data from Dandekar et al. for the WC ceramic samples show retention of substantial shear strength when shocked to stresses ca. 80 GPa.

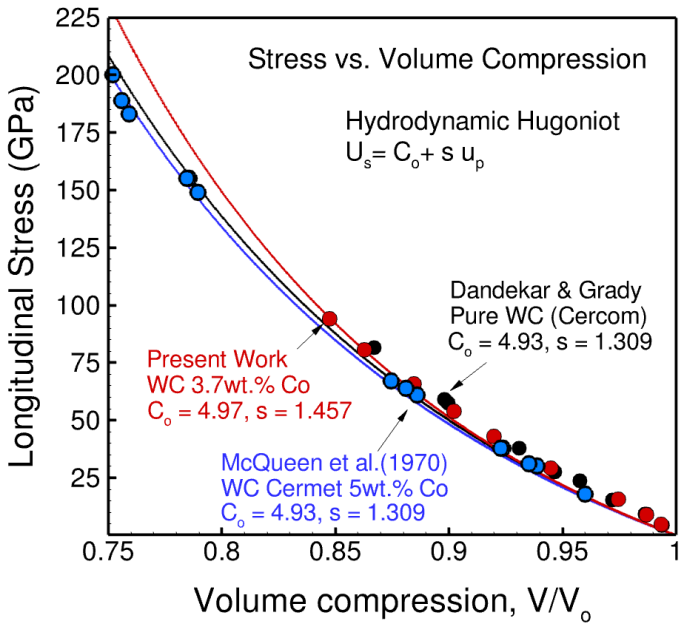

Figure 7: Longitudinal stress versus volume compression curves for cemented WC-- 3.7 wt.% cobalt (present work), WC-- 5 wt.% cobalt (McQueen et al. [15]) and pure WC ceramic (Dandekar and Grady [4]).

CONCLUSION

In the present study, shock wave experiments are conducted on General Carbide cemented tungsten carbide with 3 wt.% cobalt binder to determine its shock-induced compression behavior up to ca.100 GPa. The measured wave profiles indicate the cermet to undergo elastic-plastic deformation during its shock compression. A three-stage particle velocity profile is observed in the experiments -- an initial elastic-rise to the (HEL), an elastic-plastic ramp indicating substantial post-yield hardening, and finally a rise to the peak shocked Hugoniot state. The results of the experiments are used to determine the Hugoniot Elastic Limit (HEL), and the shock velocity (U_s) vs. particle velocity (u_p) and longitudinal stress (σ_x) vs. volume (V) Hugoniot relations for the cermet. The HEL of the material was determined to lie between 4.41 GPa and 4.58 GPa. The $U_s - u_p$ relation was determined to be $U_s = 4.97 + 1.457u_p$ for particle velocities greater than 0.75 km/s. The measured shock velocity for shocks with particle velocities less than 0.7 km/s were larger than those predicted using the linear $U_s - u_p$ Hugoniot relationship, indicating the WC cermet samples to preserve substantial shear strength in the post-yield deformation region. No phase transformation was observed up to 100 GPa.

ACKNOWLEDGEMENTS

The authors would like to thank Kurt Zimmerman, Yoshi Toyoda, and Nate Arganbright for their assistance in conducting the experiments. This work was supported by the U.S. Department of Energy/National Nuclear Security Administration (Cooperative Agreement No. DE-NA0003957).

REFERENCES

1. Zuanetti B, Wang T, Prakash V. Plate impact investigation of the dynamic response of commercial tungsten carbide under shock-induced compression and combined compression-and-shear loading. International Journal of Impact Engineering 131 200-208, 2019.

2. Gooch WA, Burkins MS, Palicka R. Ballistic development of U.S. high density tungsten carbide ceramics J. Phys. IV (10):741-746, 2000.

3. Kettenbeil C, Lovinger Z, Jiao T, Mello M, Clifton RJ, Ravichandran G. Inelastic behavior of tungsten carbide at high pressures. Journal of the Mechanics and Physics of Solids. 159, 104762, 2022.

4. Dandekar DP, Grady DE. Shock Equation of State and Dynamic Strength of Tungsten Carbide. AIP Conference Proceedings 783-786, 2002.

5. Barker LM, Hollenbach RE. Laser interferometer for measuring high-velocities of any reflecting surfaces. Journal of Applied Physics 43 (11):4669-4675, 1972.

6. Zuanetti B, Wang T, Prakash V. A compact fiber-optics based heterodyne combined normal and transverse displacement interferometer. Review of Scientific Instruments 88, 033108, 2017.

7. Yuan F, Prakash V. Plate Impact Experiments to Investigate Shock-induced Inelasticity in Westerly Granite. International Journal of Rock Mechanics and Mining Sciences. 60, 277-287, 2013.

8. Dolan DH. SAND2006-1950: Foundations of VISAR analysis. Sandial National Laboratory, Alburquerque, NM, 2006.

9. Zuanetti B, McGrane SD, Bolme CA, Prakash V. Measurement of elastic precursor decay in pre-heated aluminum films under ultra-fast laser generated shocks. Journal of Applied Physics 123 (19):195104, 2018.

10. Oniyama T, Gupta YM, Ravichandran G. Shock compression of molybdenum single crystals to 110 GPa: Elastic-plastic deformation and crystal anisotropy. Journal of Applied Physics 127 (20):205902, 2020.

11. Mandal A, Gupta YM. Elastic-plastic deformation of molybdenum single crystals shocked along [100]. Journal of Applied Physics 121 (4):045903, 2017.

12. Sunny G, Yuan F, Prakash V, Lewandowski JJ. Effect of high strain rates on peak stress in a Zr-based bulk metallic glass. Journal of Applied Physics. 104, 093522, 2008.

13. Grady D. Impact failure and fragmentation properties of tungsten carbide. International jJournal of Impact Engineering 23 307-317, 1999.

14. Appleby-Thomas GJ, Hazell PJ, Stennett C, Cooper G, Helaar K, Diederen AM. Shock propagation in a cemented tungsten carbide. Journal of Applied Physics 105 (6):064916, 2009.

15. McQueen RG, Marsh SP, Taylor JW, Fritz JN, Carter WJ. Chapter VII: The equation of state of solids from shock wave studies. High-Velocity Impact Phenomena editor(s). R. Kinslow. Academic Press, New Yok, NY, pp. 293-417, 1970.